Phys Chem Minerals (2016) 43:353–361
DOI 10.1007/s00269-016-0799-4

ORIGINAL PAPER

Phase relation of $CaSO_4$ at high pressure and temperature up to 90 GPa and 2300 K

Taku Fujii[1] · **Hiroaki Ohfuji**[1] · **Toru Inoue**[1]

Received: 8 October 2015 / Accepted: 12 January 2016 / Published online: 9 February 2016

Abstract Calcium sulfate ($CaSO_4$), one of the major sulfate minerals in the Earth's crust, is expected to play a major role in sulfur recycling into the deep mantle. Here, we investigated the crystal structure and phase relation of $CaSO_4$ up to ~90 GPa and 2300 K through a series of high-pressure experiments combined with in situ X-ray diffraction. $CaSO_4$ forms three thermodynamically stable polymorphs: anhydrite (stable below 3 GPa), monazite-type phase (stable between 3 and ~13 GPa) and barite-type phase (stable up to at least 93 GPa). Anhydrite to monazite-type phase transition is induced by pressure even at room temperature, while monazite- to barite-type transition requires heating at least to 1500 K at ~20 GPa. The barite-type phase cannot always be quenched from high temperature and is distorted to metastable $AgMnO_4$-type structure or another modified barite structure depending on pressure. We obtained the pressure–volume data and density of anhydrite, monazite- and barite-type phases and found that their densities are lower than those calculated from the PREM model in the studied P–T conditions. This suggests that $CaSO_4$ is gravitationally unstable in the mantle and fluid/melt phase into which sulfur dissolves and/or sulfate–sulfide speciation may play a major role in the sulfur recycling into the deep Earth.

Keywords Calcium sulfate · High pressure · X-ray diffraction · Raman spectroscopy · Phase transition

✉ Taku Fujii
fujii@sci.ehime-u.ac.jp

[1] Geodynamics Research Center, Ehime University, 2-5 Bunkyo-cho, Matsuyama, Ehime 790-8577, Japan

Introduction

Sulfur is one of the major magmatic volatile components and forms a variety of chemical species in the Earth's crust. Recent studies showed that the total amount of sulfur input (supplied) into subduction zone is clearly higher than the output from arc volcanoes per year, suggesting that at least a part of sulfur-bearing minerals such as sulfates and sulfides are recycled to the deep mantle (Jego and Dasgupta 2013; Evans et al. 2014). Evans et al. (2014) found that $\delta^{34}S$ values of pyrite in eclogite are close to those of seawater-derived sulfate and suggested a possibility that sulfate minerals in ocean floor sediments are subducted into substantial depths together with basalt. Anhydrite ($CaSO_4$) is one of the most abundant sulfate minerals in the crust and occurs as precipitates from hydrothermal chimneys (white smokers) in ocean floor sediments. It was also found as inclusions in diamond from Juina region, Brazil, together with chlorine-, fluorine- and carbonate-bearing mineral inclusions (Wirth et al. 2009), suggesting the sulfur recycling from crusts to mantle through subduction.

There are some experimental studies on the structural transition of $CaSO_4$ at high pressure. Stephens (1968) reported that anhydrite transforms to a high-pressure phase with a volume decrease of 4.1 % at about 2.0 GPa at room temperature, and the high-pressure phase was subsequently identified to be iso-structural to monazite ($CePO_4$) by Borg and Smith (1975). The monazite-type phase is apparently stable up to at least 28 GPa when compressed at room temperature (Bradbury and Williams 2009), while it seems to transform to another phase(s) upon heating. Chen et al. (2001) reported that anhydrite transformed to a new high-pressure phase after laser heating at about 1000 °C at 21 GPa, and after decompression to ambient condition, an orthorhombic phase was obtained based on their X-ray

diffraction measurement. On the other hand, in situ XRD observation by Crichton et al. (2005) suggested that the monazite-type phase transforms to barite-type phase at 1450 K (during heating) and 21 GPa and further transforms to a monoclinic phase with an $AgMnO_4$-type structure after quenching to room temperature. Furthermore, Ma et al. (2007) reported a phase transition of the monazite phase to another high-pressure phase, which is comparable to neither the barite-type phase nor $AgMnO_4$-type phase, after laser heating at 33.2 GPa. According to their Raman observation at room temperature, the new phase is stable at least up to 53.5 GPa and 1800 K. Moreover, a recent theoretical study by Gracia et al. (2012) proposed pressure-induced phase transitions of $CaSO_4$ from anhydrite to monazite-type phase (at 5 GPa) and then to barite or scheelite-type phases (at 8 GPa). There is, however, a discrepancy in transition pressure from the experimental observations, and the result may not be applicable to high pressure and high temperature, since the calculation was performed for 0 K. Despite these earlier reports, no consensus has been reached on the structure of high-pressure polymorphs of $CaSO_4$ and their phase relations at high pressure and high temperature.

In the present study, we conducted a series of high-pressure experiments to give constraints to the phase transitions, which may occur in oceanic crustal materials during the subduction to the deep mantle.

Experimental method

The starting material (anhydrite) used in the present experiments was obtained by annealing the calcium sulfate ($CaSO_4 \cdot nH_2O$, >99.99 %, Sigma-Aldrich Co.) at 1000 °C for 10 h. The X-ray diffraction pattern of the sample after annealing is in good agreement with JCPDS reference card no. 37-1496 for γ-$CaSO_4$, anhydrite. In situ X-ray experiments under high pressure and high temperature were performed by using two types of high-pressure apparatuses, a cubic-type multianvil press (6–6 type MA) and laser-heated diamond anvil cells (LHDAC) depending on the target pressure and temperature conditions as summarized in Table 1.

The 6–6 type MA experiments were conducted at AR-NE5C of PF-AR, KEK. The technical details of the 6–6 type MA and X-ray optical system of the beam line were described in Nishiyama et al. (2008) and Yang et al. (2014), respectively. The truncation edge length (TEL) of the second stage anvils was 6 mm, and the edge length of the pressure medium was 9 mm in run AR235 and AR240. For a higher-pressure run (AR262), the TEL of the second stage anvils of 4 mm and the edfge length of pressure medium of 7 mm were used.

The powdered sample of anhydrite and a pressure marker were enclosed in a hexagonal boron nitride (*h*-BN) sleeves and spacers (caps). The schematic illustration of the cell assembly used in the present study, which is almost identical to that used by Yang et al. (2014), is shown in Fig. 1. The temperature was measured by using a $W_{97\%}Re_{3\%}$–$W_{75\%}Re_{25\%}$ thermocouple (0.1 mm diameter) which was placed between the BN spacers of 0.3 mm thick to avoid the reaction between the sample and thermocouple. A mixture of NaCl and Au at a weight ratio of 10:1 or a mixture of

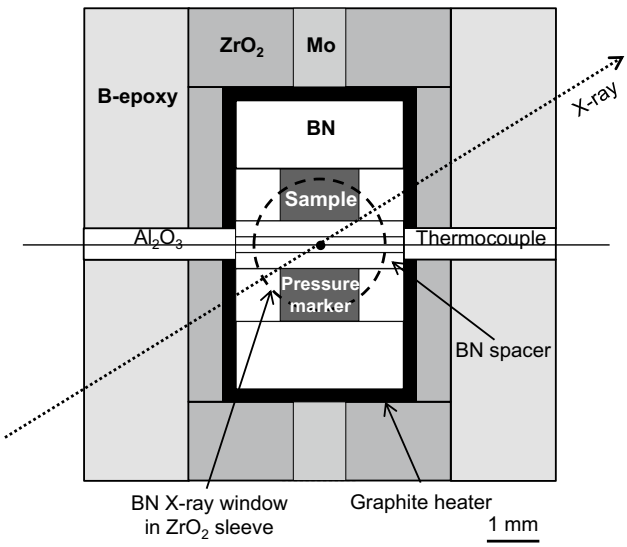

Fig. 1 Cell assembly used for the present MA experiments. The *dotted arrow line* and *circle* indicate the X-ray beam path and an X-ray window made of h-BN in the ZrO_2 sleeve

Table 1 List of experiments and their conditions

Run #	Apparatus	Pressure range (GPa)	Temperature range (K)	Pressure maker
CSSP01	DAC	9.5–38.3	300–2000	Au
CSSP02	DAC	33.0–93.1	300–2300	Au
AR235	Multianvil	~7.0	300–973	NaCl
AR240	Multianvil	~2.0	300–973[a]	NaCl
AR262	Multianvil	~3.0	300–1073	MgO

[a] Temperatures were estimated from the power–temperature relation determined in a separated run using the same high-pressure cell assembly

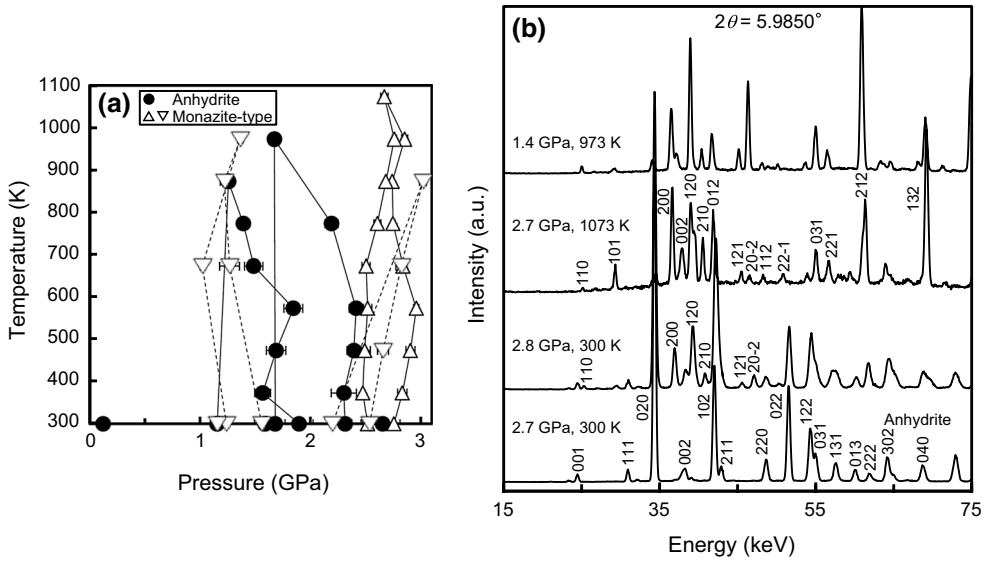

Fig. 2 P–T paths of MA experiments (**a**) and typical XRD patterns showing the phase transition from anhydrite to monazite-type phase (**b**). The *solid* and *dotted lines* in **a** indicate the heating cycle in compression and decompression paths, respectively

MgO and Au at a weight ratio of 10:1 was used as a pressure marker. The pressures were calculated using the equation of state (EoS) of NaCl (Decker 1971) and/or MgO (Jamieson et al. 1982). The lattice parameters of the sample and pressure markers were calculated using the XrayAnalysis software. In all the MA experiments, the diffraction patterns were collected with both increasing and decreasing temperature to observe the phase transition of $CaSO_4$.

The LHDAC experiments were carried out at BL10XU of SPring-8. A symmetric-type diamond cell (manufactured by Syntek Co. Ltd.) having a large X-ray window with an opening angle of 60° and diamond anvils with culet sizes of 300 and 450 μm were used. The powdered sample was compressed into a pellet form and loaded into a sample hole drilled in a pre-indented Re gasket. Both surfaces of the pelletized sample were coated with Au by the ion-sputtering, which were used as an absorbent of laser radiation and also for an internal pressure standard. No pressure medium was used to avoid any potential reactions with the sample in the present experiments. In situ X-ray diffraction measurements were taken by using a monochromatic X-ray ($\lambda = \sim 0.414$ Å) and imaging plate (IP) and CCD detectors. The each 2D diffraction image was translated to a 1D profile by azimuthal integration using IPAnalyzer software, and lattice parameters were calculated using PDIndexer software. The pressures were estimated from the EoS of Au (Tsuchiya 2003). Laser heating was conducted by using a double-sided, dual-laser ($\lambda = 1070$ nm) heating system at the beam line. The laser spots were adjusted to about 30 μm in diameter at the sample. Temperatures were measured from the both sides of the sample by spectroradiometry, and the temperature value at each input power was determined by averaging the peak temperatures of the both sides. The samples after recovery were examined by a micro-Raman spectroscopy (Photon Design Co. Ltd., Mars320) equipped with a semiconductor laser ($\lambda = 473$ nm), which was also used for in situ measurements in some runs.

Results and discussion

Figure 2a shows the *P–T* path of the multianvil experiment of run AR262 together with the phases identified by in situ XRD measurements up to 3 GPa and 1100 K. In the first and second heating at 1.8 and 2.3 GPa, no noticeable change was observed in the diffraction pattern and all the peaks were indexed with the anhydrite structure. During compression from 2.7 to 2.8 GPa (after the two cycles of heating at lower pressures), several new peaks appeared, indicating a phase transition induced by pressure. Upon heating to 1073 K and kept for ~20 min, the peaks of anhydrite gradually disappeared and were completely replaced with those of the monazite-type phase (Fig. 2b). The observed onset pressure of the phase transition from anhydrite to monazite is almost consistent with those reported in previous studies (Bradbury and Williams 2009; Ma et al. 2007). A large hysteresis was observed in the reverse (monazite phase to anhydrite) transition: The monazite phase persisted, and no anhydrite peaks appeared even after heated to 973 K and kept ~10 min at 1.4 GPa (Fig. 2b).

We, therefore, further attempted time-resolved XRD measurements during final pressure release (below 1 GPa) to detect the reverse transition. Interestingly, the diffraction peaks of the monazite phase survived until just before the

complete pressure release, and anhydrite peaks appeared when the press load reached to 0 ton as shown in Fig. 3. The diffraction peaks observed after pressure release are all indexed with anhydrite, and no residual peaks of the monazite phase were detected.

We also performed two runs using diamond anvil cell to observe further structural changes in $CaSO_4$ at higher pressure up to ~90 GPa. Figure 4 shows XRD patterns that were collected before, during and after heating in the pressure range of 12–30 GPa in run CSSP01. In the first heating to 1400 K at 13.5 GPa, no noticeable changes were observed in the diffraction pattern and all the peaks observed were indexed with the monazite-type phase. In the second heating cycle at 15–20 GPa, several new peaks appeared at 1500 K and the number and intensity of the peaks increased with increasing temperature to 1700 K. The observed new peaks can be reasonably indexed with the barite-type phase. Some major peaks of the monazite-type phase remained even after heating for ~30 min, although they almost disappear after the third heating at ~30 GPa (Fig. 4b). This is probably due to a large temperature gradient that existed vertically across the sample chamber during heating, since no thermal insulating materials were placed between the $CaSO_4$ sample and each anvil culet to avoid any potential chemical reaction with the sample.

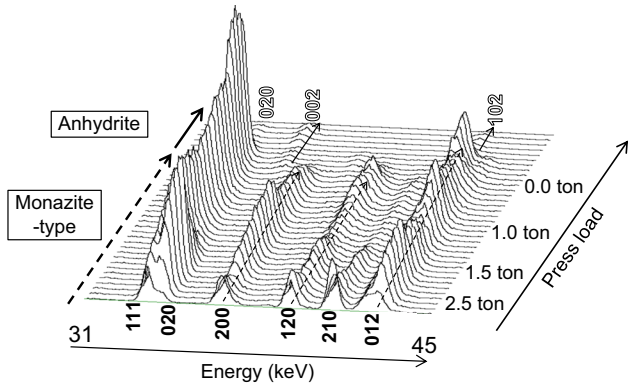

Fig. 3 Time-resolved XRD patterns during the pressure release from about 1 GPa (~2.5 ton). The press load was directly measured from the hydraulic pumping system of MAX80 press. The pressure was completely released (1 atm) when the press load reached 0.0 ton. *White* anhydrite, *black* monazite-type

Note that after quenching to room temperature (after the second heating at ~20 GPa), some of the barite peaks split and the total number of the peaks clearly increased (Fig. 4a). This is consistent with the observation of Crichton et al. (2005), in which they proposed the phase transition of the barite-type to $AgMnO_4$-type phase through a monoclinic distortion of the structural unit. It seems that the $AgMnO_4$ phase is a metastable phase that only appears at pressure around (and possibly lower than) 20 GPa, because it transformed to the barite phase during the subsequent heating and did not appear again after quenching at higher pressure (~29 GPa) (Fig. 4b). The modification from the barite to $AgMnO_4$-type structure is likely caused by the rapid drop in temperature and/or pressure upon quenching.

In the next experiment (#CSSP02), we extended the pressure range to ~90 GPa to explore further possible phase transition(s). Figure 5 shows a diffraction pattern collected

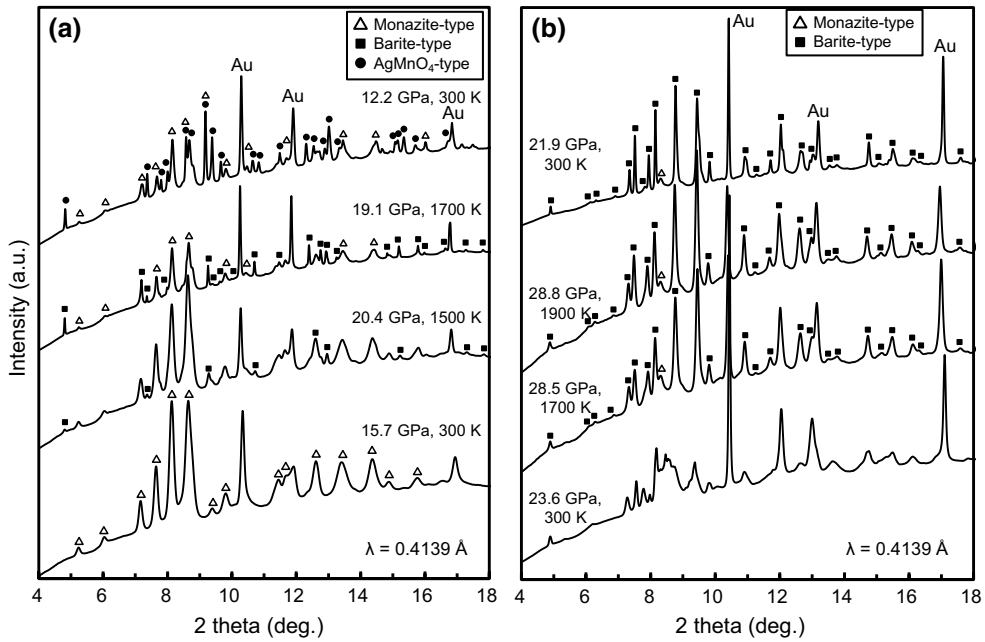

Fig. 4 Variation of the XRD patterns of $CaSO_4$ before, during and after heating at around 20 GPa (**a**) and around 30 GPa (**b**)

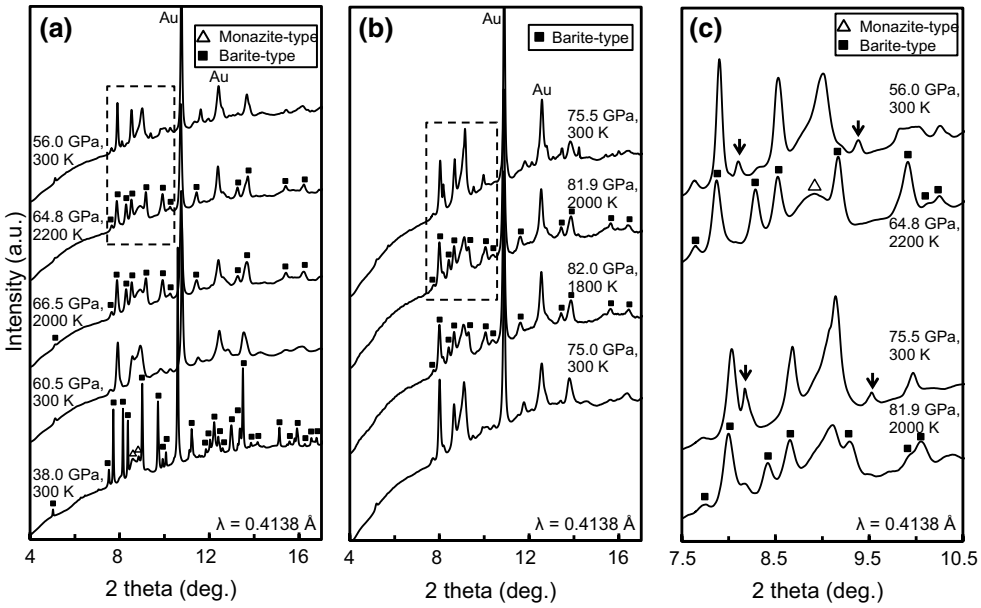

Fig. 5 Variation of the XRD patterns of $CaSO_4$ before, during and after heating at around 60 GPa (**a**) and around 80 GPa (**b**). The diffraction profiles in **c** are taken from the dotted square areas in **a** and **b**

after the first heating at ~40 GPa together with patterns collected before, during and after the second (at ~60 GPa) and third (at ~80 GPa) heating cycles. The diffraction peaks observed during heating at each pressure condition were indexed with the barite-type phase, and the barite-type phase was found to be thermodynamically stable at least, up to 93 GPa and 2300 K. However, subtle changes were found for the patterns collected after quenching to room temperature: Some of the barite peaks disappeared, while several new peaks that are explained by none of the known and potential structures, barite-type, $AgMnO_4$-type and scheelite-type appeared, as shown in Fig. 5c. This suggests that upon quenching, the barite phase transformed to a metastable phase most likely through a slight distortion of the crystal structure as is the case of the $AgMnO_4$ phase. The formation of this modified barite phase was detected only after quenching from high temperature at 60–90 GPa, but was not observed when the barite phase was compressed to above 60 GPa (from 38 GPa) at room temperature (Fig. 5a).

Figure 6 shows typical Raman spectra of the barite-type and the modified barite-type phases, which were measured after identification by in situ XRD. The spectrum of the barite phase (obtained at 60.5 GPa before heating) is in good agreement with that of the "new phase" which was found after laser heating at pressures above 33 GPa by Ma et al. (2007). Although Ma et al. (2007) did not identify the crystal structure such as by in situ XRD, the "new phase" claimed in their study must be the barite-type phase based on the present results. On the other hand, the Raman spectrum of the modified barite phase (observed after heating the barite phase) showed clearly different peaks: intense peaks at 151, 723, 744, 1190 and 1236 cm^{-1}, which are not seen for the barite phase (Fig. 6). We also collected a series

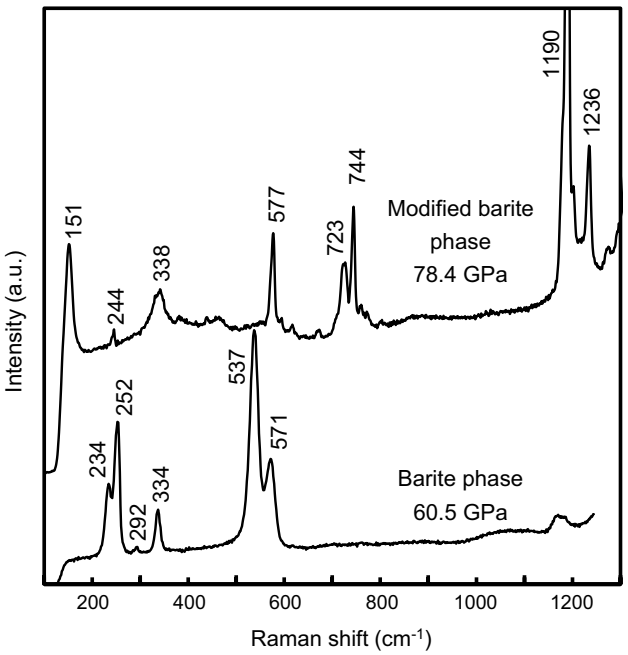

Fig. 6 Typical Raman spectra obtained from the barite-type phase before heating at 60 GPa (after compressed from 38.0 GPa at room temperature) and modified barite-type phase after heating at 2300 K at 91 GPa (pressure dropped to 78 GPa after quenching)

of Raman spectra from the modified barite phase during pressure release from 78.0 GPa to room pressure (Fig. 7). The intensity of the peaks that were originally positioned at 151 and 1236 cm^{-1} significantly decreased with decreasing pressure to ~50 GPa, while a few peaks at ~230, ~250 and ~530 cm^{-1} (at ~40 GPa) characteristic to the barite phase became intense with further pressure release, which

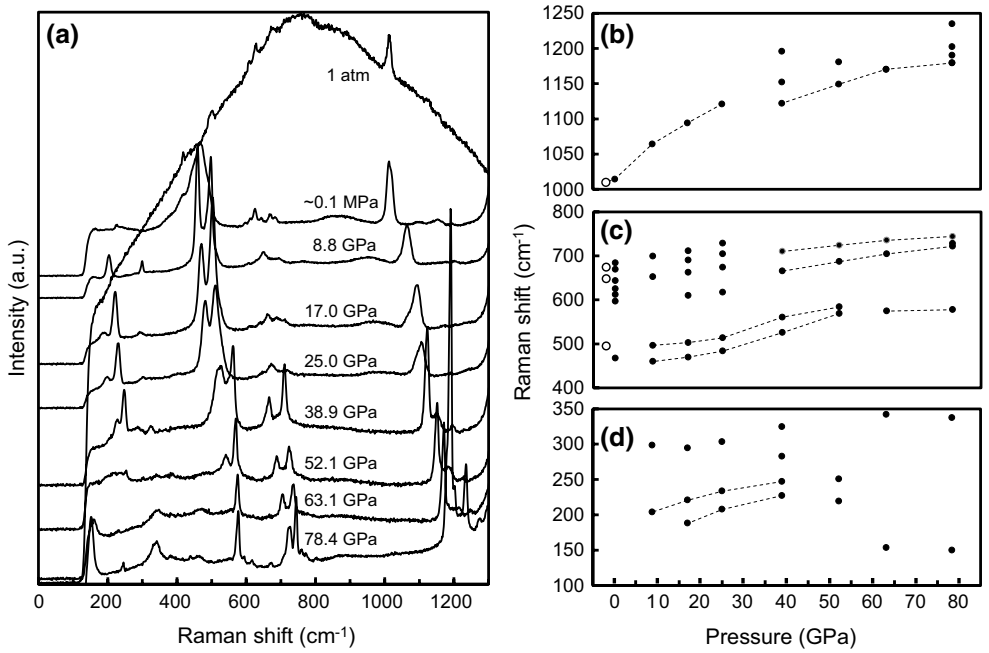

Fig. 7 Variation of Raman spectra (**a**) and Raman shift of observed peaks (**b**–**d**) during pressure release from 78.0 GPa to room pressure. The spectrum of ~0.1 MPa was collected from the sample in the DAC after complete pressure release (through a diamond anvil), while that of 1 atm was collected directly after the anvil was removed. In the latter case, a significant background increase due to fluorescence signal from the sample was observed

suggests the phase transition from the modified barite-type to barite-type phase at around 50 GPa. Another notable change was observed when the pressure was completely released: The peaks of the barite phase were quickly replaced by those of anhydrite, which suggests the phase transition from the barite-type to anhydrite without forming monazite-type phase.

Figure 8 summarizes the high-pressure and high-temperature phases of $CaSO_4$ observed in the present study. Anhydrite, monazite-type phase and barite-type phase are thermodynamically stable polymorphs in the studied PT conditions, while $AgMnO_4$-type phase and another modified barite-type phase are metastable phases that formed through the structural distortions of the barite phase only after quenching from high temperature at pressures around 20 GPa and above 55 GPa, respectively. The boundary of the pressure-induced phase transition from anhydrite to monazite is located at around 3 GPa, which is consistent with the results of previous studies (Ma et al. 2007; Bradbury and Williams 2009), although it is known to be sensitive to the hydrostaticity of the surrounding environment. Our in situ observation demonstrated for the first time that the monazite phase is not a metastable modification of anhydrite, but is certainly a stable phase at high temperature. Because of the large hysteresis of the transition pressure in compression and decompression (Fig. 2a), the slope of the phase boundary could not be discussed. The phase

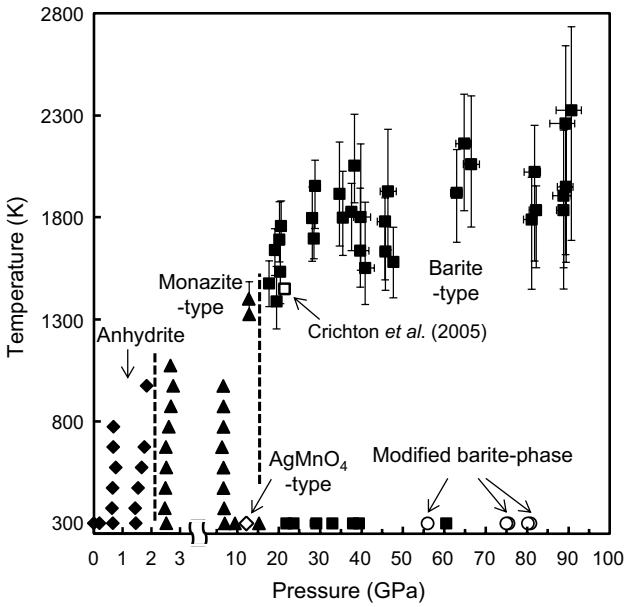

Fig. 8 Summary of the high P–T phases of $CaSO_4$ observed in the present study. $AgMnO_4$-type and modified barite-type phases form through structural distortion of the barite-type phase upon temperature quench

transition from the monazite- to barite-type phases was not observed during room temperature compression. It required heating at least to ~1500 K at ~20 GPa, suggesting that a

relatively large kinetic barrier may be involved in the transition. This is not consistent with the first-principle prediction by Gracia et al. (2012), who proposed a series of pressure-driven structural changes from anhydrite to the monazite-type phase (at 5 GPa) and then to the barite-type and/or scheelite-type phase (at 8 GPa). The discrepancy may be resulted from the temperature difference, since their calculation was performed for 0 K. In addition, scheelite phase was not observed in the preset study. In the case of ABX_4 compounds, the phase transitions from monazite to barite and to scheelite structure should require the increase in A/X and B/X cation size ratios [see Fig. 4 of Clavier et al. (2011)]. For $CaSO_4$, it is likely that the Ca/O cation size ratio increases with pressure, while the S/O size ratio remains almost unchanged, as discussed in Crichton et al. (2005). This may explain the absence of a phase transition to the scheelite phase in the studied P–T range.

In the previous experimental studies, various phases were reported as candidates for the post-monazite phase: orthorhombic phase (Chen et al. 2001), barite-type phase (Crichton et al. 2005) and another new phase (Ma et al. 2007). Chen et al. (2001) observed the phase transition from the monazite phase to a high-pressure phase by Raman spectroscopy after laser heating at 1000 °C at 21 GPa in which new Raman peaks were observed at 209, 462, 495 and 707 cm^{-1}. They also examined the product after slow pressure release by X-ray diffraction and assumed some of the observed peak that could not be indexed with the anhydrite phase to be from the partly quenched high-pressure phase. Chen et al. (2001) claimed that those diffraction peaks could be explained by an orthorhombic cell ($a = 6.602 \pm 0.005$ Å, $b = 7.759 \pm 0.007$ Å, $c = 5.970 \pm 0.007$ Å at 1 atm), which corresponds to neither the barite phase nor the $AgMnO_4$ phase. However, since such an orthorhombic phase was not observed in the decomposition product in the present study, the phase observed by Chen et al. (2001) is likely a metastable, kinetic product as noted by Crichton et al. (2005). The Raman spectrum observed after heating at 21 GPa in their study (Fig. 2c of Chen et al. 2001) is found to be comparable to that of the $AgMnO_4$-type phase observed at similar pressure conditions in this study. It therefore seems that the post-monazite phase observed by Chen et al. (2001) must have been originally the barite-type (at high temperature during heating) that was further distorted to the $AgMnO_4$-type phase upon quenching. The orthorhombic phase obtained partly in the recovered sample of Chen et al. may be a kinetic product from further distortion of the $AgMnO_4$-type structure during slow pressure release.

On the other hand, the new phase reported by Ma et al. (2007) was characterized only by Raman spectra in which, for example, five peaks were clearly detected at 212, 242, 499, 522 and 535 cm^{-1} at 33 GPa. Ma et al. (2007) compared the spectra with that of Chen et al. (2001) collected at 21 GPa and claimed that the observed new phase was different from the barite-type phase. However, there seems to be a significant misinterpretation about the phase identification, because the phase obtained by Chen et al. (2001) is probably not the barite-type, but $AgMnO_4$-type, as discussed above. Indeed, the Raman spectra shown by Ma et al. (2007) (in Fig. 5 of their paper) are well comparable to those of the barite-type phase observed in this study (Figs. 6, 7a), suggesting that the "new phase" described by Ma et al. (2007) is most likely the barite-type phase. Taking into consideration these facts, we conclude that the post-monazite phase is certainly the barite-type, which is found to be stable in a wide pressure and temperature range at least up to 93 GPa and 2300 K.

The pressure–volume (P–V) data obtained through in situ observation of anhydrite, monazite- and barite-type phases are shown in Fig. 9. Basically, the volume data were calculated from diffraction patterns collected after heating (annealing) to exclude the influence of stress accumulated during compression/decompression at room temperature. Our P–V data of monazite match well with the previous data reported by Crichton et al. (2005) but deviated from those of Ma et al. (2007) and Bradbury and Williams (2009). Since the volume data of those latter studies were obtained during room temperature compression (without annealing at high temperature), the deviation may be caused by the influence of deviatoric stress or from poor peak fitting (particularly, the quality of the corresponding

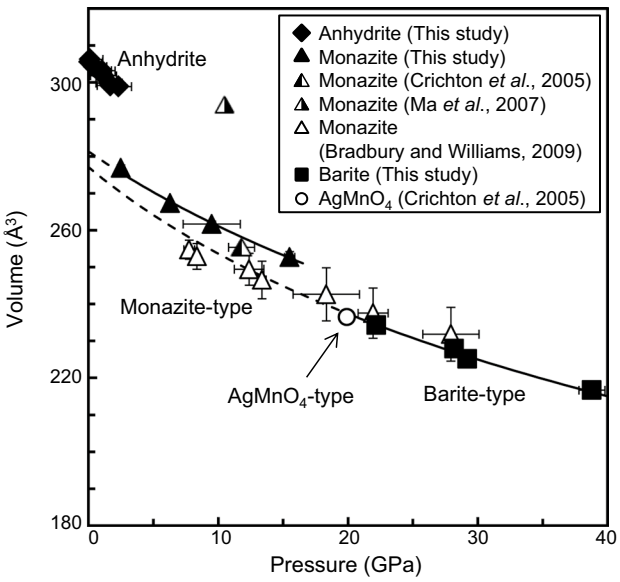

Fig. 9 P–V data of anhydrite, monazite- and barite-type phase as summarized in Table 2 in comparison with those of previous studies. The *solid* and *dashed lines* are the compression curves for monazite- and barite-type phases, respectively, obtained by BM-EoS fitting

Table 2 Lattice parameters, volume and density calculated for monazite-type and barite-type phase at each pressure condition

Run #	Pressure (GPa)	Phase	*a*-axis (Å)	*b*-axis (Å)	*c*-axis (Å)	*b*-angle (°)	*V* (Å^3)	Density (g/cm^3)
AR262035	2.5 (1)	Monazite	6.590 (84)	6.816 (5)	6.331 (8)	103.167 (59)	276.85 (83)	3.26 (2)
AR235024	6.3 (2)	Monazite	6.492 (3)	6.740 (2)	6.263 (6)	102.721 (46)	267.32 (43)	3.41(1)
CSSP01001	9.5 (22)	Monazite	6.465 (9)	6.697 (2)	6.188 (8)	102.442 (50)	261.63 (78)	3.46 (2)
CSSP01011	15.5 (4)	Monazite	6.333 (18)	6.620 (5)	6.161 (17)	102.001 (101)	252.64 (156)	3.58 (4)
CSSP01038	22.2 (2)	Barite	6.319 (4)	7.521 (5)	4.928 (7)		234.19 (63)	3.86 (2)
CSSP01046	28.2 (4)	Barite	6.260 (3)	7.468 (3)	4.873 (4)		227.81 (35)	3.97 (1)
CSSP02017	29.2 (4)	Barite	6.236 (2)	7.428 (3)	4.858 (3)		225.03 (28)	4.02 (1)
CSSP02028	38.8 (10)	Barite	6.157 (2)	7.345 (3)	4.790 (2)		216.61 (27)	4.18 (1)

diffraction pattern of Ma et al. 2007 is considerably poor). Table 2 summarizes the lattice parameters and volume of the monazite- and barite-type phases calculated from the each data point of Fig. 9. In order to determine the equation of state (EoS) of the unquenchable high-pressure phases, we first fitted the data to the following modified Birch–Murnaghan EoS that is used to constrain the elastic parameters of a phase for which the zero-pressure volume is unobtainable (Jeanloz 1981) by following the procedure used by Bradbury and Williams (2009).

$$P = 3(1+2g)^{\frac{5}{2}}\alpha^5 K_0 \times \left\{\left(\alpha^2-1\right)/2\left[1+\xi\left(1-\alpha^2\right)+\cdots\right] + \alpha^2\left[1+2\xi\left(1-\alpha^2\right)+\cdots\right]g+\cdots\right\} \quad (1)$$

$$\xi = 3/4\left(4-K_0'\right) \quad (2)$$

$$g = 1/2\left\{\left(\rho/\rho^*\right)^{\frac{2}{3}}-1\right\} \quad (3)$$

$$\alpha = \left(\rho^*/\rho\right)^{\frac{1}{3}} \quad (4)$$

Here, ρ^* is an arbitrary reference density, K_0 is the bulk modulus, and K_0' is its pressure derivative. We extrapolated the zero-pressure volume of the monazite and barite phases using Eqs. (1)–(4), in which K_0' was fixed at 4. The V_0 values obtained for the monazite and barite phases are 281.1 (5) and 277.3 (40) Å^3, respectively. The *P*–*V* data of the each phase were then fitted separately with the third-order Birch–Murnaghan EoS as follows,

$$P = 3/2K_{T0}\left[(V_0/V)^{\frac{7}{3}}-(V_0/V)^{\frac{5}{3}}\right] \times \left\{1+3/4\left(K_{T0}'-4\right)\left[(V_0/V)^{\frac{2}{3}}-1\right]\right\} \quad (5)$$

where V_0, K_{T0} and K_{T0}' are unit cell volume, isothermal bulk modulus and its pressure derivative, respectively, at ambient conditions. K_{T0}' was fixed at 4. The monazite-type phase gave $K_{T0} = 115$ (4) GPa, while the barite-type phase gave $K_{T0} = 97$ (14) GPa. The bulk modulus of the monazite phase is different from the value [$K_{T0} = 151$ (21) GPa] reported by Bradbury and Williams (2009) who obtained a series of P–T data during room temperature compression to 28 GPa. The K_{T0} of Bradbury and Williams (2009) may have been overestimated due to non-negligible deviatoric stress. The obtained bulk modulus of the barite-type phase is likely underestimated (because lower than that of monazite) due to relatively large scattering of the fitted data points and the lack of data at low-pressure region (Fig. 9), which also resulted in a larger error in V_0 extrapolation as shown above. A further in situ diffraction study is necessary to obtain reliable elastic parameters and to precisely

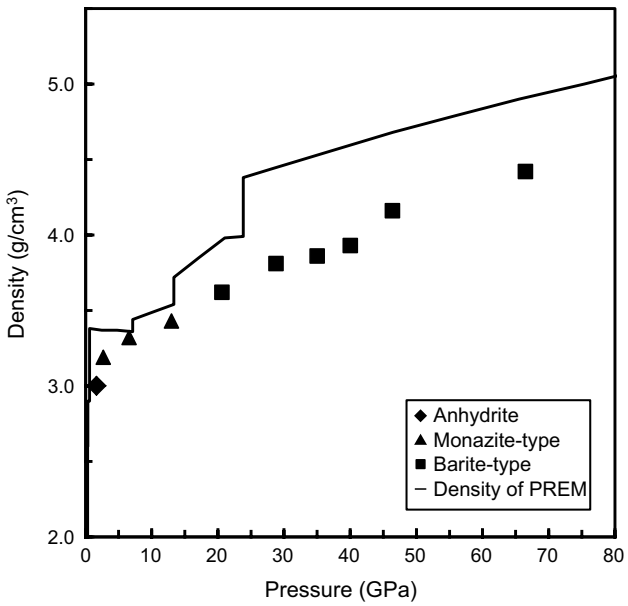

Fig. 10 Densities of the thermodynamically stable $CaSO_4$ polymorphs against pressure in comparison with that of the PREM model. Each density data of the $CaSO_4$ phases is calculated directly from the unit cell volume determined by the XRD pattern at the temperature close to the corresponding mantle depth (considering the standard geotherm)

determine the volume reduction accompanied by the monazite–barite phase transition.

Figure 10 shows a plot of densities of $CaSO_4$ phases that were calculated from the volume data obtained in this study against pressure together with the density variation of the PREM model. The densities of anhydrite and its high-pressure form are lower than those of the PREM, although the density of the monazite-type phase is close to the PREM in the range of 7–13 GPa. This suggests that $CaSO_4$ is gravitationally unstable and will not be solely subducted to the deep mantle. However, since recent mineralogical and geochemical studies suggested the sulfur recycling into the mantle (Wirth et al. 2009; Jego and Dasgupta 2013; Evans et al. 2014), it is important to understand how and in which form sulfur is entrained to the deep mantle. Fluid/melt phase into which sulfur dissolves at high pressure and temperature as well as the sulfate–sulfide speciation may play a significant role in the transportation process as recently suggested by Jego and Dasgupta (2013, 2014).

Conclusion

This study demonstrates high-pressure transition and phase relation of $CaSO_4$ up to ~90 GPa and 2300 K on the basis of the result obtained by in situ X-ray diffraction and Raman spectroscopy. We confirmed that monazite-type and barite-type phases are thermodynamically stable polymorphs of anhydrite (ambient phase) at high pressure and high temperature. The phase transition from anhydrite to monazite phase is induced by pressure at ~3 GPa even at room temperature, while monazite to barite transition is activated at high temperature (>1500 K at ~20 GPa). The barite-type phase cannot always be quenched from high temperature and is distorted to $AgMnO_4$-type structure (at 12–20 GPa) or another modified barite structure (at >55 GPa) upon quenching.

Acknowledgments The authors thank Prof. T Irifune for the technical support and suggestions. We also thank Dr. W. Crichton and an anonymous reviewer for their critical reviews and comments that helped to improve the present report. This study was supported by JSPS KAKENHI Grant Number 26287138 to H. O.

References

Borg IY, Smith DK (1975) A high pressure polymorph of $CaSO_4$. Contrib Mineral Petrol 50:127–133

Bradbury SE, Williams Q (2009) X-ray diffraction and infrared spectroscopy of monazite-structured $CaSO_4$ at high pressures: implications for shocked anhydrite. J Phys Chem Solids 70:134–141

Chen CC, Liu LG, Lin C, Yang YJ (2001) High-pressure phase transformation in $CaSO_4$. J Phys Chem Solids 62:1293–1298

Clavier N, Podor R, Dacheux N (2011) Cristal chemistry of the monazite structure. J Eur Ceram Soc 31:941–976

Crichton WA, Parise JB, Sytle SM, Grzechnik A (2005) Evidence for monazite-, barite-, and $AgMnO_4$ (distorted barite)-type structures of $CaSO_4$ at high pressure and temperature. Am Mineral 90:22–27

Decker DL (1971) High-pressure equation of state for NaCl, KCl, and CsCl. J Appl Phys 42:3239

Evans KA, Tomlins AG, Cliff J, Fiorentini ML (2014) Insights into subduction zone sulfur recycling from isotopic analysis of eclogite-hosted sulfides. Chem Grol 365:1–19

Gracia L, Beltran A, Errandonea D, Andres J (2012) $CaSO_4$ and its pressure-induced phase transitions. A density functional theory study. Inorg Chem 51:1751–1759

Jamieson JC, Fritz JN, Manghnani MH (1982) Pressure measurement at high temperature in X-ray diffraction studies: gold as a primary standard. High Press Res 67:27–48

Jeanloz R (1981) Finite-strain equation of state for high-pressure phases. Geophys Res Lett 8(12):1219–1222

Jego S, Dasgupta R (2013) Fluid-present melting of sulfide-bearing ocean-crust: experimental constraints on the transport of sulfur from subducting slab to mantle wedge. Geochimica et Cosmo Chimica Acta 110:106–134

Jego S, Dasgupta R (2014) The fate of sulfur during fluid-present melting of subducting basaltic crust at variable oxygen fugacity. J Petrol 55(6):1019–1050

Ma YM, Zhou Q, He Z, Li FF, Cui QL, Zou GT (2007) High-pressure and high-temperature study of the phase transition in anhydrite. J Phys Condens Matter 19:425221

Nishiyama N, Wang Y, Sanehira T, Irifune T, Rivers ML (2008) Development of the multi-anvil assembly 6-6 for DIA and D-DIA type high-pressure apparatuses. High Press Res 28:307–314

Stephens DR (1968) The hydrostatic compression of eight rocks. J Geophys Res 69:2967–2978

Tsuchiya T (2003) First-principles prediction of the P–V–T equation of state of gold and the 660-km discontinuity in Earth's mantle. J Geophys Res 108:2462

Wirth R, Kaminsky F, Matsyuk S, Schreiber A (2009) Unusual micro- and nano-inclusions in diamonds from the Juina Area, Brazil. Earth Planet Sci Lett 268:292–303

Yang C, Inoue T, Yamada A, Kikegawa T, Ando J (2014) Equation of state and phase transition of antigorite under high pressure and high temperature. Phys Earth Planet Inter 228:56–62